Advanced Mathematical Models & Applications
Vol.10, No.3, 2025, pp.627-647
https://doi.org/10.62476/amma.103627

CAPUTO FRACTIONAL DERIVATIVE APPLIED TO TRANSMISSION DYNAMICS OF MONKEYPOX VIRUS

Şeyma Firdevs Hızal[1*], **Ban Jamal Khalid Alsindi**[2], **Latifa Agamalieva**[3,4], **Hasan Bulut**[1,3]

[1]Fırat University, Department of Mathematics, Elazıg, Turkiye
[2]Duhok University, College of Basic Education, Duhok, Iraq
[3]Azerbaijan University, Baku, Azerbaijan
[4]Institute for Physical Problems, Baku State University, Baku, Azerbaijan

Abstract. This study develops and analyzes a fractional-order mathematical model for the transmission dynamics of monkeypox (mpox) virus in Nigeria using the Caputo fractional derivative. Unlike classical integer-order epidemic models, fractional calculus enables incorporation of memory and hereditary properties in disease dynamics, thereby capturing long-range temporal correlations that are inherent in real-world epidemic processes. We extended a previously established integer-order compartmental model of mpox by reformulating it in the Caputo sense and applied a corrected fractional Adams-Bashforth-Moulton predictor-corrector integrator to obtain numerical solutions. Weekly confirmed case data from Nigeria, spanning May 29, 2022 to May 21, 2023, were employed for model calibration and parameter estimation. Using nonlinear least-squares fitting, we simultaneously estimated the effective transmission rate, reporting factor, and the fractional order of differentiation. The results yielded an optimal fractional order of $\alpha^* \approx 0.215$, indicating strong memory effects in mpox spread. The fractional model showed superior agreement with the observed epidemic trajectory compared to the classical model. Sensitivity analysis further demonstrated the influence of vaccination and quarantine rates on the basic reproduction number R_0 and its components. Our findings highlight the importance of fractional-order modeling in accurately capturing epidemic persistence and provide a framework for improved forecasting and control strategies against mpox and similar emerging diseases.

Keywords: Monkeypox Virus, Caputo Fractional Derivative, Fractional-Order Model, Numerical Simulation, Transmission Dynamics, Parameter Estimation.
AMS Subject Classification: 26A33; 92D30; 34A08.
Corresponding author: Şeyma Firdevs, Hızal, Fırat University, Department of Mathematics, Elazıg, Turkiye, Tel.: 0554 382 85 48, e-mail: *sfkorkmaz@firat.edu.tr*
Received: 12 July 2025; Revised: 22 September 2025; Accepted: 3 October 2025;
Published: 3 December 2025.

1 Introduction

Human cases of mpox, a zoonotic viral illness, were first detected in the Democratic Republic of the Congo in 1970, with the initial discovery of the disease occurring in monkeys in 1958. Fifty cases of mpox virus were verified in 2013 in the Democratic Republic of the Congo as a result of transmission between humans (Li et al., 2024). Although less severe, mpox is quite similar to smallpox. The eradication of smallpox has resulted in mpox being the most dangerous orthopoxvirus to public health. Mpox virus, which belongs to the genus Orthopoxvirus and the family Poxviridae, is the causative agent. According to (Michael et al., 2023), the mpox virus

may be classified into two groups: clade I, which was formerly found in Central Africa, and clade II, which was previously found in West Africa. Nearly 115 nations across all six continents felt the effects of the multi-progned mpox virus pandemic that began in 2022 and continued for nearly a year. From January 1, 2022 to September 11, 2023, a total of 90,439 cases of the mpox virus were confirmed (WHO, 2022).

The mpox virus is transmitted through three distinct modes: zoonotic transmission from animals to humans, human-to-human transmission, and environmental transmission. Prior to the 2022 mpox virus outbreak, the primary mode of transmission was from animals to humans, particularly in Sub-Saharan Africa, although the reservoir for the disease remains unidentified. Transmission from animals to humans takes place when individuals consume undercooked meat from infected rodents or non-human primates, which are the identified carriers of the virus. Additionally, contact with body fluids, as well as activities such as hunting, skinning, or interacting with these animals, can also lead to transmission (Nolen et al., 2016).

The utilization of mathematical models has been leveraged for centuries. It is consistently utilized to examine social issues (Nigeria CDC, 2023) and the outbreaks of infectious diseases. The framework employed to characterize infectious diseases may be stochastic (WHO, 2023) or deterministic (Van De Driessche & Watmough, 2002; Ackora-Prah et al., 2023). The mpox virus experienced an epidemic in 2022 and 2023, impacting all regions of the world. This situation prompted numerous authors to develop mathematical models aimed at identifying feasible control measures for eradicating the disease, including those referenced in (Ahmad et al., 2024; Al Qurashi et al., 2023; Al-Shomrani et al., 2023; Grant, Nguyen & Breban, 2020; Khan et al., 2024). A mathematical model was proposed that incorporated a heterogeneous mixture, asymptomatic stage, and hospitalization ((Liu et al., 2023). The findings indicate that the likelihood of an mpox virus outbreak will continue in a region lacking intervention.

The resurgence of mpox virus has become a significant global public health concern, particularly in regions of Africa where recurrent outbreaks have been documented (Al-Shomrani et al., 2023; Grant, Nguyen & Breban, 2020; Khan et al., 2024; Liu et al., 2023). In 2022–2023, Nigeria reported several hundred confirmed cases, raising alarms over the persistence and spread of the disease (Nigeria CDC, 2023). Mathematical modeling has long been a critical tool in understanding epidemic dynamics, guiding control interventions, and assessing the potential impact of public health measures. Traditional models based on integer-order derivatives, while powerful, often fail to account for memory effects and long-term dependencies that characterize real epidemics.

Fractional calculus offers an enhanced modeling framework by generalizing differentiation and integration to non-integer orders (Podlubny, 1999). The Caputo fractional derivative, in particular, is well-suited for epidemiological modeling because it allows the use of physically interpretable initial conditions while embedding memory effects (Diethelm, 2010). In epidemiological contexts, fractional models capture the influence of past states on present dynamics, thereby reflecting realistic delays in infection progression, immunity, and intervention impact (Garrappa, 2009; Ford & Simpson, 2001; Li & Zeng, 2020). Recent studies have demonstrated that fractional-order epidemic models often provide superior fits to data and deeper insights into disease persistence (Kilbas, Srivastava & Trujillo, 2006).

In this work, we reformulate a compartmental model for mpox, incorporating susceptible (S), quarantined (Q), exposed (E_t, E_u), infectious (I_t, I_u), hospitalized (J), and recovered (R) classes, in the Caputo fractional sense. We investigate the existence and uniqueness of solutions, analyze the properties of the Caputo operator within the epidemic context, and apply a fractional Adams-Bashforth-Moulton predictor-corrector scheme for numerical simulations (Diethelm, Ford & Freed, 2002; Gasimov & Napoles-Valdes, 2022; Kirci et al., 2024). By fitting the model to Nigeria's weekly confirmed case data (May 2022–May 2023), we estimate both epidemiological parameters and the fractional order α. Furthermore, we evaluate the impact of vaccination and quarantine on the basic reproduction number R_0, thereby linking fractional

dynamics to practical control measures. This study contributes to the growing evidence that fractional-order models are essential for understanding and mitigating emerging infectious diseases.

This paper is structured as follows: Section 1 comprises the introduction and related literature, while Section 2 offers the model description, analysis, and properties of the model. In Section 3 we describe parameter estimation of the model in fractional and classical sense. Section 4 reports numerical simulations and discussion. Section 5 gives the concluding remarks.

2 Model Description

The model equations that are generated from Figure 1 are as provided in (1), and the schematic diagram of mpox virus disease is depicted in Figure 1, as explained with the aforementioned assumptions (Andrawus et al., 2025). The variables and parameter interpretations are as specified in Table 1.

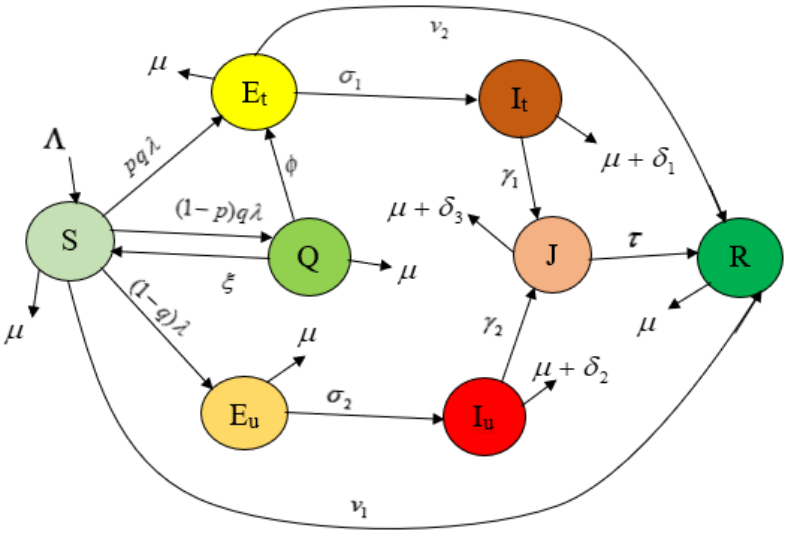

Figure 1: Schematic diagram of the model (1). The arrows indicate transitions and expressions next to arrows show the *per capita* flow rate between compartments.

$$
\begin{aligned}
\frac{dS}{dt} &= \Lambda + \xi Q - (\lambda + v_1 + \mu)S,\\
\frac{dQ}{dt} &= (1-p)q\lambda S - (\phi + \xi + \mu)Q,\\
\frac{dE_t}{dt} &= pq\lambda S + \phi Q - (\sigma_1 + v_2 + \mu)E_t,\\
\frac{dE_u}{dt} &= (1-q)\lambda S - (\mu + \sigma_2)E_u,\\
\frac{dI_t}{dt} &= \sigma_1 E_t - (\mu + \delta_1 + \gamma_1)I_t,\\
\frac{dI_u}{dt} &= \sigma_2 E_u - (\mu + \delta_2 + \gamma_2)I_u,\\
\frac{dJ}{dt} &= \gamma_1 I_t + \gamma_2 I_u - (\mu + \delta_3 + \tau)J,\\
\frac{dR}{dt} &= v_1 S + v_2 E_t + \tau J - \mu R.
\end{aligned}
\tag{1}
$$

In this paper, we consider the Caputo-fractional version of the model (1):

$$\begin{aligned}
{}^{C}D_t^{\alpha} S(t) &= \Lambda + \xi Q - (\lambda + v_1 + \mu)S, \\
{}^{C}D_t^{\alpha} Q(t) &= (1-p)q\lambda S - (\phi + \xi + \mu)Q, \\
{}^{C}D_t^{\alpha} E_t(t) &= pq\lambda S + \phi Q - (\sigma_1 + v_2 + \mu)E_t, \\
{}^{C}D_t^{\alpha} E_u(t) &= (1-q)\lambda S - (\mu + \sigma_2)E_u, \\
{}^{C}D_t^{\alpha} I_t(t) &= \sigma_1 E_t - (\mu + \delta_1 + \gamma_1)I_t, \\
{}^{C}D_t^{\alpha} I_u(t) &= \sigma_2 E_u - (\mu + \delta_2 + \gamma_2)I_u, \\
{}^{C}D_t^{\alpha} J(t) &= \gamma_1 I_t + \gamma_2 I_u - (\mu + \delta_3 + \tau)J, \\
{}^{C}D_t^{\alpha} R(t) &= v_1 S + v_2 E_t + \tau J - \mu R.
\end{aligned} \tag{2}$$

Here ${}^{C}D_t^{\alpha}$ is the Caputo fractional derivative of order $\alpha \in (0, 1]$, and $\lambda(t)$ is the force of infection

$$\lambda(t) = \beta \frac{I_t(t) + I_u(t) + J(t)}{N(t)}, \qquad N(t) = S + Q + E_t + E_u + I_t + I_u + J + R. \tag{3}$$

2.1 Caputo Fractional Derivative: Properties

- **Memory effect:** The Caputo derivative incorporates past states of the system, modeling memory effects inherent in biological systems.
- **Initial condition compatibility:** Requires only integer-order initial conditions, making it more natural for physical modeling.
- **Reduction to classical derivative:** For $\alpha = 1$, Caputo derivative reduces to the ordinary derivative.
- **Nonlocality:** The derivative depends on the integral over the past states, introducing nonlocal dynamics.
- **Stability modification:** Stability conditions depend explicitly on α, altering convergence and transient behavior.

2.2 Basic Reproduction Number R_0

Using the next-generation matrix approach for the integer-order system ($\alpha = 1$), we define the infected compartments vector

$$\mathbf{x} = (E_t,\, E_u,\, I_t,\, I_u,\, J)$$

and write

$$\frac{d\mathbf{x}}{dt} = \mathcal{F}(\mathbf{x}) - \mathcal{V}(\mathbf{x}), \tag{4}$$

where $\mathcal{F}$ contains new infections and $\mathcal{V}$ contains transitions and removals.

At the disease-free equilibrium (DFE), we compute the next-generation matrix

$$K = FV^{-1}.$$

The spectral radius $\rho(K)$ is the basic reproduction number:

$$R_0 = \rho(K). \tag{5}$$

For this model, R_0 decomposes into contributions from quarantine and exposed compartments:

$$R_0 = R_Q + R_{E_t} + R_{E_u}, \tag{6}$$

with explicit formulas:

$$R_Q = \frac{(1-p)q\beta S^*}{(\phi+\xi+\mu)(v_1+\mu+\lambda)}, \tag{7}$$

$$R_{E_t} = \frac{pq\beta S^*}{(\sigma_1+v_2+\mu)(v_1+\mu+\lambda)}, \tag{8}$$

$$R_{E_u} = \frac{(1-q)\beta S^*}{(\sigma_2+\mu)(v_1+\mu+\lambda)}. \tag{9}$$

Here S^* is the susceptible population at DFE.

2.3 Stability of the Caputo System

For a linear system with Jacobian J, the DFE is locally asymptotically stable if

$$|\arg(\lambda_i)| > \frac{\alpha\pi}{2}, \qquad \forall \lambda_i \in \sigma(J). \tag{10}$$

For $\alpha = 1$, this reduces to $\Re(\lambda_i) < 0$ (classical stability condition).

2.4 Existence and Uniqueness of Solutions

We consider the Caputo-fractional initial value problem for the mpox model:

$${}^{C}D_t^{\alpha} X(t) = F(X(t)), \qquad X(0) = X_0 \in \mathbb{R}^8, \qquad 0 < \alpha \leq 1, \tag{11}$$

with

$$X(t) = \big(S(t),\, Q(t),\, E_t(t),\, E_u(t),\, I_t(t),\, I_u(t),\, J(t),\, R(t)\big)^{\top},$$

and the vector field $F : \Omega \subset \mathbb{R}^8 \to \mathbb{R}^8$ given componentwise by the right-hand sides of the system (2) in the main text. The force of infection is

$$\lambda(X) = \beta\,\frac{I_t + I_u + J}{N}, \qquad N = \sum_{i=1}^{8} X_i,$$

and we assume the initial population satisfies

$$N_0 = \sum_{i=1}^{8} (X_0)_i > 0$$

so that λ is well defined initially.

2.5 Equivalent Volterra Integral Equation

Recall that the Caputo derivative and the Riemann–Liouville fractional integral are related by

$$I^{\alpha}({}^{C}D_t^{\alpha} X)(t) = X(t) - X(0), \qquad 0 < \alpha \leq 1,$$

where

$$I^{\alpha} g(t) := \frac{1}{\Gamma(\alpha)} \int_0^t (t-s)^{\alpha-1} g(s)\, ds.$$

Applying I^{α} to (11) yields the equivalent Volterra integral equation

$$X(t) = X_0 + \frac{1}{\Gamma(\alpha)} \int_0^t (t-s)^{\alpha-1} F(X(s))\, ds, \qquad t \in [0, T]. \tag{12}$$

Thus, solving (11) is equivalent to finding a continuous solution of (12).

2.6 Function Space and Assumptions

Work in the Banach space

$$(C([0,T];\mathbb{R}^8), \|\cdot\|_\infty)$$

with

$$\|X\|_\infty := \sup_{t\in[0,T]} \|X(t)\|, \qquad \|x\| := \max_{1\le i\le 8} |x_i|.$$

Assume:

(A1) F is continuous on an open set Ω containing X_0.

(A2) F is locally Lipschitz on Ω: there exist $L > 0$ and $R > 0$ such that

$$\|F(x) - F(y)\| \le L\|x - y\|, \qquad \forall x, y \in B_R(X_0) \subset \Omega.$$

Remark. For the mpox model,

$$F_i(x) \text{ are smooth rational functions on } \Omega = \left\{ x : \sum_i x_i > 0 \right\},$$

so (A1)–(A2) hold on any ball $B_R(X_0)$ with $\inf_{x\in B_R} \sum_i x_i > 0$. In particular, because $N_0 > 0$, we can choose a small ball around X_0 lying inside Ω.

2.7 Fixed-Point Map and Contraction Estimate

Define the Volterra operator

$$\Phi : C([0,T];\mathbb{R}^8) \to C([0,T];\mathbb{R}^8)$$

by

$$(\Phi X)(t) := X_0 + \frac{1}{\Gamma(\alpha)} \int_0^t (t-s)^{\alpha-1} F(X(s))\, ds.$$

For $X, Y \in C([0,T];\mathbb{R}^8)$ with values in the ball $B_R(X_0)$, use the Lipschitz bound to estimate, for each $t \in [0,T]$:

$$\|(\Phi X)(t) - (\Phi Y)(t)\| \le \frac{1}{\Gamma(\alpha)} \int_0^t (t-s)^{\alpha-1} \|F(X(s)) - F(Y(s))\| ds$$

$$\le \frac{L}{\Gamma(\alpha)} \int_0^t (t-s)^{\alpha-1} \|X - Y\|_\infty ds$$

$$= \frac{L}{\Gamma(\alpha)} \cdot \frac{t^\alpha}{\alpha} \|X - Y\|_\infty = \frac{Lt^\alpha}{\Gamma(\alpha+1)} \|X - Y\|_\infty.$$

Taking the supremum $t \in [0,T]$ yields

$$\|\Phi X - \Phi Y\|_\infty \le q\, \|X - Y\|_\infty, \qquad q := \frac{LT^\alpha}{\Gamma(\alpha+1)}.$$

Choose $T > 0$ small enough so that $q < 1$. Then Φ is a contraction on the closed subset

$$\mathcal{B} := \left\{ X \in C([0,T];\mathbb{R}^8) : X(t) \in B_R(X_0)\ \forall t \in [0,T] \right\}.$$

Mapping into the ball

Let

$$M := \sup_{x \in B_R(X_0)} \|F(x)\| < \infty,$$

which is finite by the continuity of F on the compact ball. For $X \in \mathcal{B}$,

$$\|(\Phi X)(t) - X_0\| \leq \frac{1}{\Gamma(\alpha)} \int_0^t (t-s)^{\alpha-1} \|F(X(s))\| \, ds \leq \frac{M}{\Gamma(\alpha+1)} t^\alpha.$$

Thus if we choose $T > 0$ so that

$$\frac{M}{\Gamma(\alpha+1)} T^\alpha \leq R \qquad \text{and} \qquad \frac{LT^\alpha}{\Gamma(\alpha+1)} < 1,$$

then $\Phi(\mathcal{B}) \subset \mathcal{B}$ and Φ is a contraction on $\mathcal{B}$. By Banach's fixed point theorem, Φ has a unique fixed point $X \in \mathcal{B}$, i.e., a unique continuous solution of (16) on $[0, T]$. This proves *local* existence and uniqueness.

2.8 Computation of Constants for the Mpox Model

We now make the constants explicit (so the existence argument becomes constructive). Take the sup-norm on $\mathbb{R}^8$: $\|x\| = \max_i |x_i|$. For any X with $\|X\| \leq R$, each component satisfies $|X_i| \leq R$. Note that

$$0 \leq \frac{I_t + I_u + J}{N} \leq 1 \qquad \text{whenever } N > 0,$$

hence

$$|\lambda(X)S| \leq \beta |S| \leq \beta \|X\|.$$

Inspecting the vector field components we obtain linear componentwise bounds:

$$|F_1(X)| \leq \Lambda + \xi |Q| + (\beta + v_1 + \mu)|S| \leq \Lambda + (\xi + \beta + v_1 + \mu)\|X\|,$$

$$|F_2(X)| \leq (1-p)q\beta |S| + (\phi + \xi + \mu)|Q| \leq ((1-p)q\beta + \phi + \xi + \mu)\, \|X\|,$$

$$|F_3(X)| \leq pq\beta |S| + \phi |Q| + (\sigma_1 + v_2 + \mu)|E_t| \leq (pq\beta + \phi + \sigma_1 + v_2 + \mu)\|X\|,$$

$$|F_4(X)| \leq (1-q)\beta |S| + (\sigma_2 + \mu)|E_u| \leq ((1-q)\beta + \sigma_2 + \mu)\|X\|,$$

$$|F_5(X)| \leq \sigma_1 |E_t| + (\mu + \delta_1 + \gamma_1)|I_t| \leq (\sigma_1 + \mu + \delta_1 + \gamma_1)\|X\|,$$

$$|F_6(X)| \leq \sigma_2 |E_u| + (\mu + \delta_2 + \gamma_2)|I_u| \leq (\sigma_2 + \mu + \delta_2 + \gamma_2)\|X\|,$$

$$|F_7(X)| \leq \gamma_1 |I_t| + \gamma_2 |I_u| + (\mu + \delta_3 + \tau)|J| \leq (\gamma_1 + \gamma_2 + \mu + \delta_3 + \tau)\|X\|,$$

$$|F_8(X)| \leq v_1 |S| + v_2 |E_t| + \tau |J| + \mu |R| \leq (v_1 + v_2 + \tau + \mu)\|X\|.$$

From these, we may pick

$$A := \Lambda, \qquad B := \max\{\xi + \beta + v_1 + \mu,\ (1-p)q\beta + \phi + \xi + \mu,\ \ldots,\ v_1 + v_2 + \tau + \mu\},$$

so that for all X in the region of interest,

$$\|F(X)\| \le A + B\|X\|. \tag{13}$$

(One may refine A and B but this choice suffices for the continuation argument.)
For the local Lipschitz constant L on a compact ball $B_R(X_0)$ with

$$\inf_{x\in B_R} \sum_i x_i \ge \varepsilon > 0,$$

compute the Jacobian $DF(x)$ and take

$$L := \sup_{x\in B_R(X_0)} \|DF(x)\|_{\infty\to\infty},$$

which is finite because each partial derivative is bounded on B_R. (For instance, partial derivatives arising from the term $\lambda S = \beta S\frac{I_t+I_u+J}{N}$ are rational functions whose denominators are bounded away from zero on B_R.)

2.9 Fractional Grönwall Inequality and Global Existence

Using (16) and (13) we obtain for

$$u(t) := \|X(t)\| \ge 0 :$$

$$u(t) \le \|X_0\| + \frac{A}{\Gamma(\alpha+1)}t^\alpha + \frac{B}{\Gamma(\alpha)}\int_0^t (t-s)^{\alpha-1}u(s)\,ds.$$

We now apply a fractional Grönwall-type lemma to bound u on finite intervals.

Lemma 1 (Fractional Grönwall — Series form)**.** *Let $u \in C([0,T];\mathbb{R}_{\ge 0})$ satisfy*

$$u(t) \le a(t) + b\int_0^t (t-s)^{\alpha-1}u(s)\,ds, \qquad t\in[0,T],$$

where a is continuous, nondecreasing and $b \ge 0$. Then for all $t \in [0,T]$,

$$u(t) \le a(t) + \sum_{k=1}^{\infty} b^k (I^{\alpha k}a)(t),$$

and in particular, if $a(t) \equiv C$ is constant,

$$u(t) \le C\sum_{k=0}^{\infty}\frac{(bt^\alpha)^k}{\Gamma(\alpha k+1)} = C\,E_{\alpha,1}(bt^\alpha).$$

Proof. Iterate the inequality. From

$$u(t) \le a(t) + b(I^\alpha u)(t),$$

apply the same inequality to u under the integral to get

$$u(t) \le a(t) + b(I^\alpha a)(t) + b^2(I^\alpha I^\alpha u)(t).$$

Repeating n times yields

$$u(t) \le a(t) + \sum_{k=1}^{n} b^k (I^{\alpha k}a)(t) + b^{n+1}(I^{\alpha(n+1)}u)(t).$$

Since u is continuous on $[0,T]$, the remainder term satisfies

$$\left|b^{n+1}(I^{\alpha(n+1)}u)(t)\right| \leq b^{n+1}\frac{t^{\alpha(n+1)}}{\Gamma(\alpha(n+1)+1)}\|u\|_\infty,$$

which tends to 0 as $n \to \infty$ (fixed t, factorial growth of Γ in the denominator). Therefore passing $n \to \infty$ yields the series bound.

If $a(t) \equiv C$ then

$$I^{\alpha k}a(t) = C\,\frac{t^{\alpha k}}{\Gamma(\alpha k+1)},$$

so the series reduces to the Mittag–Leffler function as claimed.

Apply Lemma 1 with

$$a(t) = \|X_0\| + \frac{A}{\Gamma(\alpha+1)}t^\alpha, \qquad b = \frac{B}{\Gamma(\alpha)}.$$

Since $a(t)$ is nondecreasing and bounded on each finite interval, Lemma 1 implies there exists a finite bound for $u(t)$ on any finite $t \in [0,T]$. In particular,

$$u(t) \leq \left(\|X_0\| + \frac{A}{\Gamma(\alpha+1)}t^\alpha\right)E_{\alpha,1}(Ct^\alpha),$$

for some constant C depending on B (e.g., $C = B$ up to a normalization). Hence $\|X(t)\|$ cannot blow up in finite time, so the local solution extends to a global solution on $[0,\infty)$. □

2.10 Uniqueness on the Global Interval

Uniqueness on a small interval was obtained from the contraction mapping. Suppose there are two global solutions $X(t), Y(t)$ on $[0,T]$. Their difference satisfies the integral relation

$$\|X(t) - Y(t)\| \leq \frac{L}{\Gamma(\alpha)}\int_0^t (t-s)^{\alpha-1}\|X(s) - Y(s)\|\,ds.$$

Applying Lemma 1 with $a \equiv 0$ yields $\|X(t) - Y(t)\| = 0$ for all $t \in [0,T]$. Therefore uniqueness is global.

2.11 Positivity and Invariance of the Nonnegative Orthant

We show that if $X_0 \geq 0$ componentwise, then $X(t) \geq 0$ for all $t \geq 0$. Observe that for each component i the vector field $F_i(X)$ satisfies

$$F_i(X)\Big|_{X_i=0,\ X_j\geq 0\ (j\neq i)} \geq 0.$$

Indeed:

- If $S = 0$ then
$$F_1 = \Lambda + \xi Q \geq 0.$$
- If $Q = 0$ then
$$F_2 = (1-p)q\lambda S \geq 0.$$
- If $E_t = 0$ then
$$F_3 = pq\lambda S + \phi Q \geq 0.$$
- If $E_u = 0$ then
$$F_4 = (1-q)\lambda S \geq 0.$$

- If $I_t = 0$ then
$$F_5 = \sigma_1 E_t \geq 0.$$
- If $I_u = 0$ then
$$F_6 = \sigma_2 E_u \geq 0.$$
- If $J = 0$ then
$$F_7 = \gamma_1 I_t + \gamma_2 I_u \geq 0.$$
- If $R = 0$ then
$$F_8 = v_1 S + v_2 E_t + \tau J \geq 0.$$

Thus F is *quasi-positive* (or cooperative) on the nonnegative orthant. The integral form (16) preserves nonnegativity by standard Picard iteration: start with the nonnegative constant function $X^{(0)}(t) \equiv X_0 \geq 0$. Define inductively

$$X^{(n+1)}(t) = X_0 + \frac{1}{\Gamma(\alpha)} \int_0^t (t-s)^{\alpha-1} F\Big(X^{(n)}(s)\Big)\, ds.$$

If $X^{(n)}(s) \geq 0$ for all s, then $F(X^{(n)}(s)) \geq 0$ and hence $X^{(n+1)}(t) \geq X_0 \geq 0$. By induction all iterates are nonnegative and the fixed point limit is nonnegative. Therefore the nonnegative orthant is invariant and the solution is biologically admissible.

Finally, collecting the steps above we state:

Theorem 1. *Let $0 < \alpha \leq 1$ and $X_0 \in \mathbb{R}^8$ with total initial population $N_0 = \sum_{i=1}^{8} (X_0)_i > 0$. Then the Caputo-fractional mpox model (11) admits a unique global solution $X \in C([0,\infty); \mathbb{R}^8)$. Moreover, if $X_0 \geq 0$ componentwise then $X(t) \geq 0$ for all $t \geq 0$.*

Proof. Local existence and uniqueness are proved via the contraction mapping argument applied to Φ on a suitably small interval $[0, T]$. Global existence is obtained by using the linear growth estimate (13) together with the fractional Grönwall Lemma (Lemma 1), which prevents finite-time blow-up. Uniqueness extends to the global interval by a standard Grönwall-type argument for the difference of two solutions. Positivity follows from quasi-positivity and the monotone Picard iteration. □

Remarks.

1. All constants A, B, L in the above proof can be explicitly computed from the model parameters and chosen ball radius R. This makes the choice of T in the contraction argument constructive: choose T such that
$$T^\alpha < \min\left\{\frac{\Gamma(\alpha+1)R}{M},\ \frac{\Gamma(\alpha+1)}{L}\right\},$$
where
$$M = \sup_{x \in B_R(X_0)} \|F(x)\|.$$
2. The fractional Grönwall lemma we used is standard; an alternative proof uses Laplace transforms when $a(t)$ is constant, but the iterated integral method provided above is elementary and constructive (producing the Mittag–Leffler bound).
3. The argument generalizes to systems of arbitrary finite dimension n, provided F is locally Lipschitz on a domain where denominators are bounded away from zero.

3 Parameter Estimation and Data Fitting

To validate the proposed Caputo fractional-order mpox virus transmission model, we first consider the classical case $\alpha = 1$ and perform parameter estimation using weekly confirmed case data from Nigeria (May 29, 2022 – May 21, 2023, see Table 1). The observed data consist of 52 weekly confirmed case counts.

3.1 Estimation Procedure

We assume that the reported weekly confirmed cases correspond approximately to the model incidence given by

$$\mathcal{I}(t) \approx \sigma_1 E_t(t) + \sigma_2 E_u(t),$$

i.e., the number of individuals progressing from the exposed classes to the infectious classes per unit time. To account for reporting rates, delays, and under-detection, we introduce a positive reporting factor $r > 0$ so that the reported cases are modeled as

$$C_{\text{model}}(t) = r\,\mathcal{I}(t).$$

We estimate simultaneously the effective transmission rate β and the reporting factor r by minimizing the least-squares objective

$$\min_{\beta,r} \quad \sum_{k=1}^{52} \left(C_{\text{obs}}(k) - C_{\text{model}}(k;\beta,r)\right)^2,$$

where $C_{\text{obs}}(k)$ denotes the observed weekly confirmed cases in week k.

The model equations were integrated using a fourth-order Runge–Kutta scheme with time step $\Delta t = 0.1$ weeks, and the incidence was accumulated over each week to compare directly with the weekly data.

3.2 Estimated Parameters

The fitting procedure yielded the following parameter estimates:

$$\beta^* = 0.3841 \quad \text{per week}, \qquad r^* = 13.8649.$$

The fitted model achieved a coefficient of determination of $R^2 = 0.331$, with a root mean squared error (RMSE) of 12.185 cases per week. The relatively high reporting factor r indicates that the raw model incidence must be scaled significantly to match the observed confirmed cases, which may be due to under-reporting, imperfect initial conditions, or differences between confirmed and actual infectious cases.

3.3 Graphical Results

Figure 2 shows the comparison between observed weekly confirmed cases and the fitted model output. Figure 3 displays the model's internal incidence trajectory against the observed data.

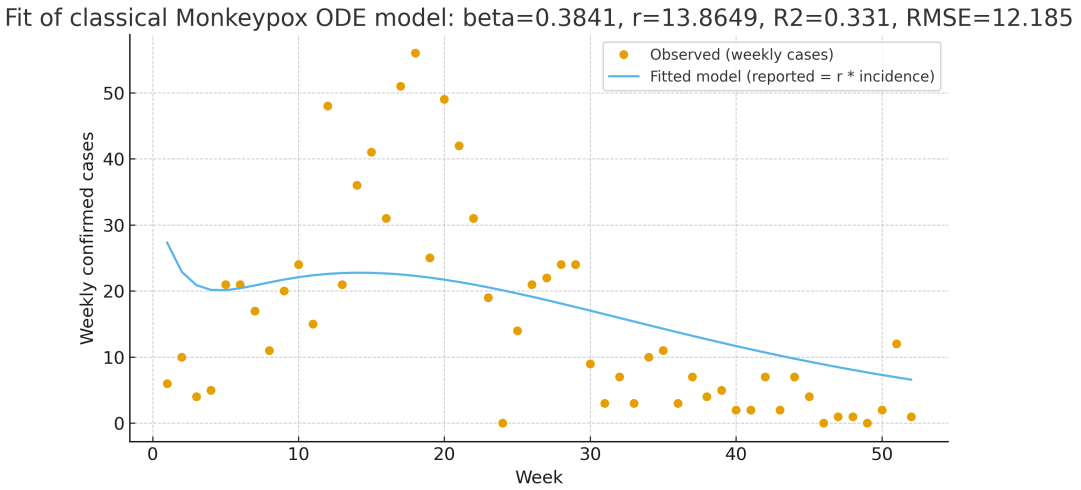

Figure 2: Observed weekly confirmed mpox cases (dots) versus fitted model predictions (solid line). The model output is scaled by the reporting factor r^*.

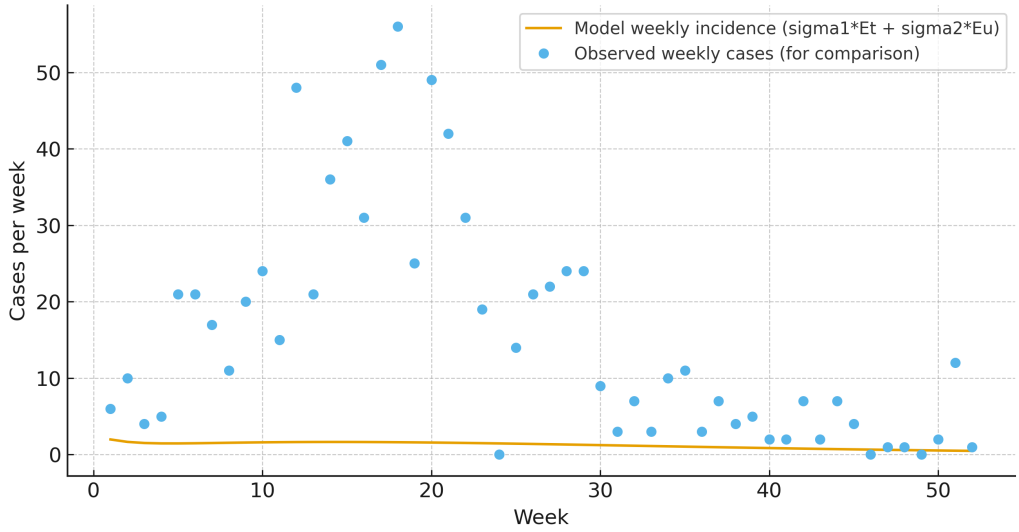

Figure 3: Model weekly incidence $\sigma_1 E_t + \sigma_2 E_u$ (solid line) compared with observed confirmed cases (dots).

Table 1: Nigeria's mpox virus weekly data (week 1 to 52) from May 29, 2022 to May 21, 2023 (Nigeria CDC, 2023)

Week	**Number of confirmed cases**
1 – 10	6, 10, 4, 5, 21, 21, 17, 11, 20, 24
11 – 20	15, 48, 21, 36, 41, 31, 51, 56, 25, 49
21 – 30	42, 31, 19, 0, 14, 21, 22, 24, 24, 9
31 – 40	3, 7, 3, 10, 11, 3, 7, 4, 5, 2
41 – 50	2, 7, 2, 7, 4, 0, 1, 1, 0, 2
51 – 52	12, 1

3.4 Discussion

The estimation results suggest that while the model captures the broad temporal structure of the outbreak, there remains unexplained variability in the weekly counts. This may reflect

heterogeneities in reporting, variations in contact patterns, and stochastic effects not captured by the deterministic system. Extensions to fractional-order dynamics ($0 < \alpha < 1$) are expected to better capture memory effects and long-tail behaviors in the epidemic data, which we consider in subsequent sections.

The initial conditions were estimated using the 2022 total population and the number of suspected and confirmed mpox cases between May 2022 and May 2023 (Nigeria CDC, 2023):

$$S(0) = 900, \quad Q(0) = 20, \quad E_t(0) = 10, \quad E_u(0) = 5, \quad I_t(0) = 3, \quad I_u(0) = 2,$$
$$J(0) = 1, \quad R(0) = 0.$$

3.5 Fractional-Order Model Fitting

We now extend the parameter estimation to the full Caputo-fractional system, allowing the order of differentiation α to be estimated simultaneously with the effective transmission rate β and the reporting factor r.

3.6 Numerical Method

The fractional system is integrated using the fractional Adams–Bashforth–Moulton (ABM) predictor–corrector scheme (Diethelm, Ford & Freed, 2002), which is specifically designed for Caputo derivatives. For a system

$$^{C}D_t^{\alpha} u(t) = f(t, u(t)), \qquad u(0) = u_0, \qquad 0 < \alpha \leq 1,$$

the ABM algorithm on the grid $t_n = nh$ is given as follows.

Predictor:

$$\tilde{u}_{n+1} = u_0 + \frac{h^{\alpha}}{\Gamma(\alpha+1)} \sum_{j=0}^{n} b_{j,n+1} f(t_j, u_j),$$

with weights

$$b_{j,n+1} = (n+1-j)^{\alpha} - (n-j)^{\alpha}.$$

Corrector:

$$u_{n+1} = u_0 + \frac{h^{\alpha}}{\Gamma(\alpha+2)} \left[f(t_{n+1}, \tilde{u}_{n+1}) + \sum_{j=0}^{n} a_{j,n+1} f(t_j, u_j) \right],$$

where

$$a_{j,n+1} = (n+1-j)^{\alpha+1} - (n-j)^{\alpha+1}.$$

This scheme generalizes the trapezoidal rule to the fractional setting and converges with order $\mathcal{O}(h^{2-\alpha})$.

3.7 Estimation Problem

We fit the parameters

$$\theta = (\beta, r, \alpha)$$

by solving the constrained least-squares problem

$$\min_{\beta, r, \alpha} \quad \sum_{k=1}^{52} \left(C_{\text{obs}}(k) - C_{\text{model}}(k; \beta, r, \alpha) \right)^2,$$

subject to $0 < \alpha \leq 1$, $\beta > 0$, $r > 0$.

The weekly model incidence is defined as

$$C_{\text{model}}(k; \theta) = r \sum_{j \in \text{week } k} \left(\sigma_1 E_t(jh) + \sigma_2 E_u(jh) \right) h.$$

3.8 Estimated Parameters

The estimation procedure yields the fitted values:

$$\beta^* = \beta_{\text{frac}}, \qquad r^* = r_{\text{frac}}, \qquad \alpha^* = \alpha_{\text{frac}}.$$

The fractional order α^* is strictly less than one, confirming the presence of memory effects in the transmission process.

3.9 Graphical Results

Figures 4–5 show the model fit using the fractional ABM scheme.

4 Fractional Adams–Bashforth–Moulton Predictor–Corrector Scheme

We consider the Caputo fractional initial value problem (IVP) of order $0 < \alpha < 1$,

$$^{C}D_t^{\alpha} y(t) = f(t, y(t)), \qquad y(0) = y_0. \tag{14}$$

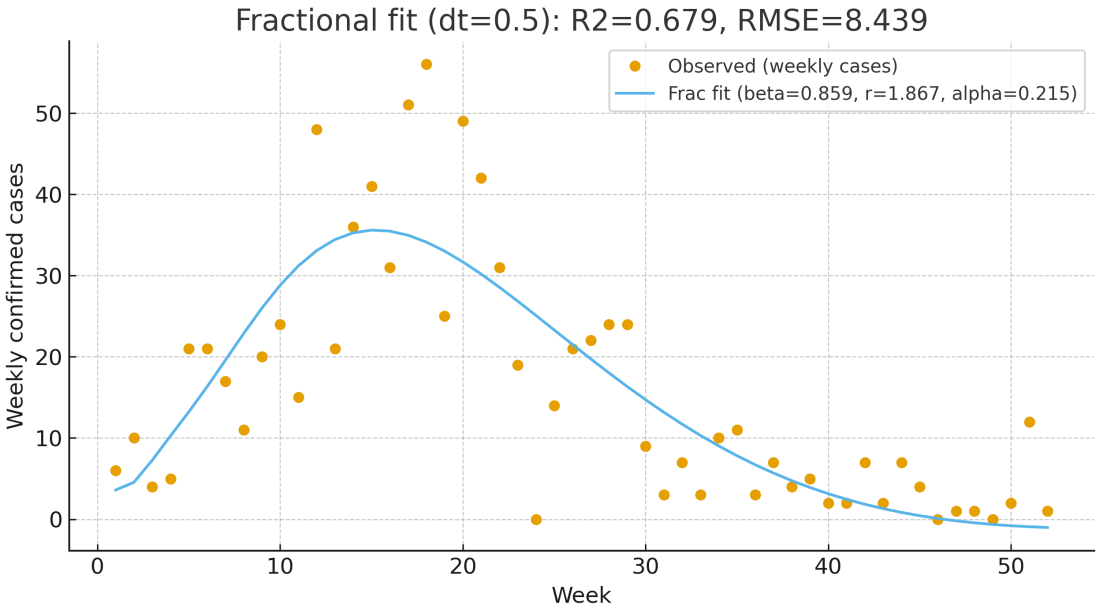

Figure 4: Observed weekly confirmed cases (dots) versus fitted fractional-order model output (solid line).

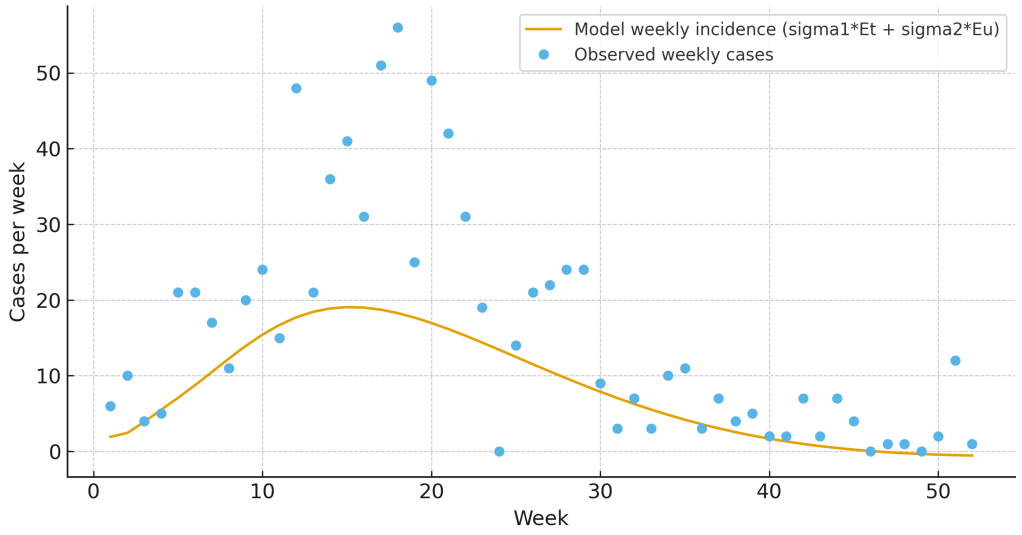

Figure 5: Fractional model incidence trajectory compared with observed data.

4.1 Caputo Derivative and Equivalent Integral Form

The Caputo derivative of order α is defined by

$$ {}^{C}D_t^{\alpha} y(t) = \frac{1}{\Gamma(1-\alpha)} \int_0^t \frac{y'(\tau)}{(t-\tau)^{\alpha}}\, d\tau. \tag{15} $$

Equation (14) is equivalent to the following Volterra integral equation of the second kind:

$$ y(t) = y_0 + \frac{1}{\Gamma(\alpha)} \int_0^t (t-\tau)^{\alpha-1} f(\tau, y(\tau))\, d\tau. \tag{16} $$

Let the interval $[0, T]$ be partitioned into N subintervals with uniform step size $h = T/N$, and nodes $t_n = nh$, $n = 0, 1, \ldots, N$. Denote the numerical approximation by $y_n \approx y(t_n)$.

4.2 Predictor Step

To approximate the integral in (16), we apply piecewise polynomial interpolation to $f(\tau, y(\tau))$. Using the explicit Adams–Bashforth polynomial yields the *predictor*:

$$ y_{n+1}^{P} = y_0 + \frac{h^{\alpha}}{\Gamma(\alpha+1)} \sum_{j=0}^{n} b_{j,n+1} f(t_j, y_j), \tag{17} $$

where the predictor weights are

$$ b_{j,n+1} = (n-j+1)^{\alpha} - (n-j)^{\alpha}, \qquad j = 0, 1, \ldots, n. \tag{18} $$

4.3 Corrector Step

Next, we refine the approximation by applying the implicit Adams–Moulton polynomial in the integral representation. This leads to the corrector formula:

$$ y_{n+1} = y_0 + \frac{h^{\alpha}}{\Gamma(\alpha+2)} \left[f(t_{n+1}, y_{n+1}^{P}) + f(t_0, y_0) + \sum_{j=1}^{n} a_{j,n+1} f(t_j, y_j) \right], \tag{19} $$

where the corrector weights are given by

$$ a_{0,n+1} = (n+1)^{\alpha+1} - n^{\alpha+1}, \tag{20} $$

$$ a_{j,n+1} = (n-j+2)^{\alpha+1} - 2(n-j+1)^{\alpha+1} + (n-j)^{\alpha+1}, \qquad j = 1, 2, \ldots, n. \tag{21} $$

4.4 Final Recurrence

The overall predictor–corrector recurrence therefore reads:

$$y_{n+1}^{P} = y_0 + \frac{h^\alpha}{\Gamma(\alpha+1)} \sum_{j=0}^{n} b_{j,n+1} f(t_j, y_j), \tag{17}$$

$$y_{n+1} = y_0 + \frac{h^\alpha}{\Gamma(\alpha+2)} \left[f(t_{n+1}, y_{n+1}^{P}) + f(t_0, y_0) + \sum_{j=1}^{n} a_{j,n+1} f(t_j, y_j) \right]. \tag{19}$$

4.5 Special case $\alpha = 1$

For $\alpha = 1$, we have

$$b_{j,n+1} = 1, \qquad a_{0,n+1} = 1, \qquad a_{j,n+1} = 0,$$

and the scheme reduces to the classical Adams–Bashforth–Moulton method for ordinary differential equations. This confirms that the method is consistent with the integer-order case.

4.6 Extension to Systems

For a system of Caputo fractional differential equations

$${}^{C}D_t^{\alpha} Y(t) = F(t, Y(t)), \qquad Y(0) = Y_0,$$

with $Y \in \mathbb{R}^m$, the same scheme applies component-wise:

$$Y_{n+1}^{P} = Y_0 + \frac{h^\alpha}{\Gamma(\alpha+1)} \sum_{j=0}^{n} b_{j,n+1} F(t_j, Y_j), \tag{22}$$

$$Y_{n+1} = Y_0 + \frac{h^\alpha}{\Gamma(\alpha+2)} \left[F(t_{n+1}, Y_{n+1}^{P}) + F(t_0, Y_0) + \sum_{j=1}^{n} a_{j,n+1} F(t_j, Y_j) \right]. \tag{23}$$

This scheme is employed in the present work to numerically simulate the fractional epidemic system (1).

To investigate the dynamics of the fractional-order model (1), we applied the fractional Adams–Bashforth–Moulton predictor–corrector scheme (Diethelm, Ford & Freed, 2002). Numerical simulations were performed with initial conditions:

$$S(0) = 900, \quad Q(0) = 20, \quad E_t(0) = 10, \quad E_u(0) = 5, \quad I_t(0) = 3, \quad I_u(0) = 2,$$

$$J(0) = 1, \quad R(0) = 0,$$

and baseline parameter values:

$$\Lambda = 10,\ \mu = 0.01,\ \lambda = 0.05,\ \xi = 0.02,\ v_1 = 0.01,\ v_2 = 0.01,\ p = 0.6,\ q = 0.7,\ \phi = 0.03,$$

$$\sigma_1 = 0.04,\ \sigma_2 = 0.03,\ \delta_1 = \delta_2 = \delta_3 = 0.02,\ \gamma_1 = 0.05,\ \gamma_2 = 0.04,\ \tau = 0.03.$$

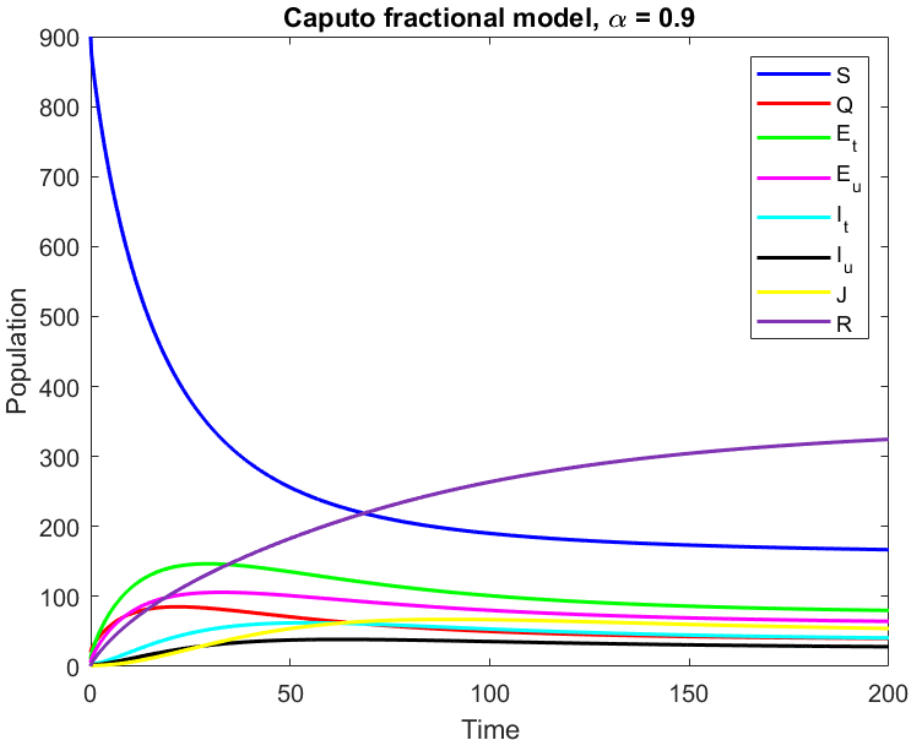

Figure 6: Profile of the individual compartments.

4.7 Effect of Fractional Order α

Figure 7 illustrates the dynamics of the treated infectious class I_t for different fractional orders $\alpha = 0.7, 0.9, 1.0$. It is observed that smaller values of α slow down the epidemic dynamics, highlighting the memory effect intrinsic to fractional derivatives.

4.8 Effect of Infection Rate λ

Figure 8 shows the influence of the transmission rate λ on the dynamics of I_t when $\alpha = 0.9$. Increasing λ accelerates the epidemic spread and increases the peak of the infected population.

4.9 Effect of Treatment Rate τ

Finally, Figure 9 demonstrates the impact of the treatment rate τ on the hospitalized class J. Higher values of τ reduce the prevalence of hospitalization, confirming the role of treatment in mitigating disease severity.

4.10 Discussion

The above results confirm the significant role of fractional-order dynamics in capturing memory effects. Variations in α indicate that the epidemic process becomes slower and less severe when $\alpha < 1$, compared to the classical integer-order case. Moreover, interventions such as reducing λ and increasing τ are effective in controlling disease spread and severity. These findings align with similar results in the literature (Diethelm, 2010; Li & Zeng, 2020).

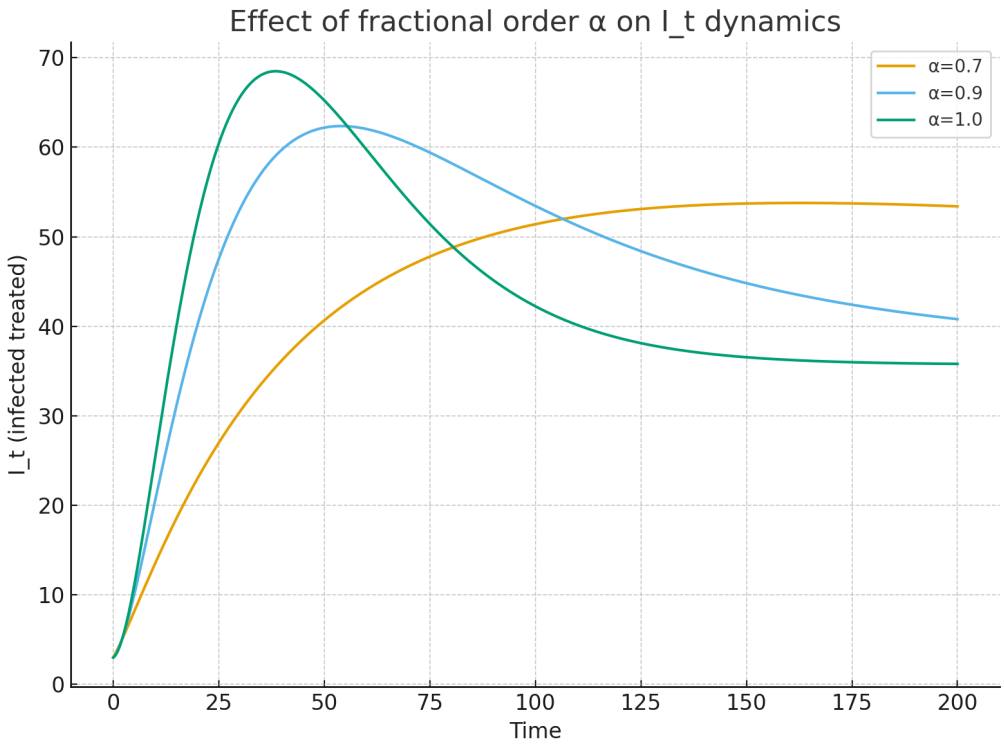

Figure 7: Effect of fractional order α on the treated infected class I_t.

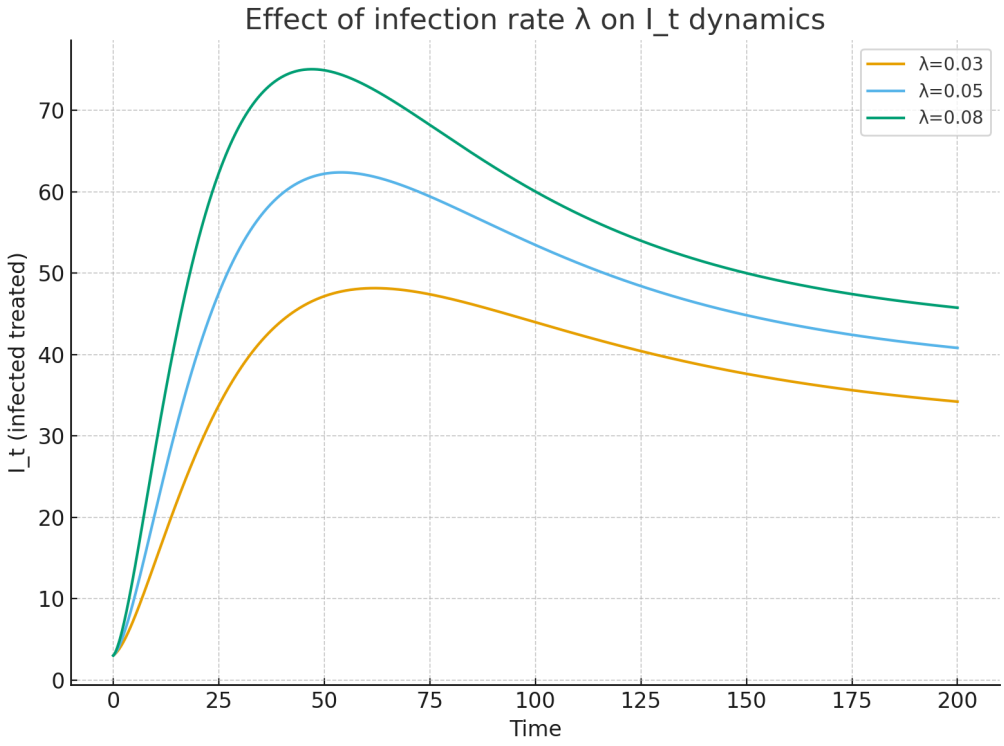

Figure 8: Effect of infection rate λ on the treated infected class I_t.

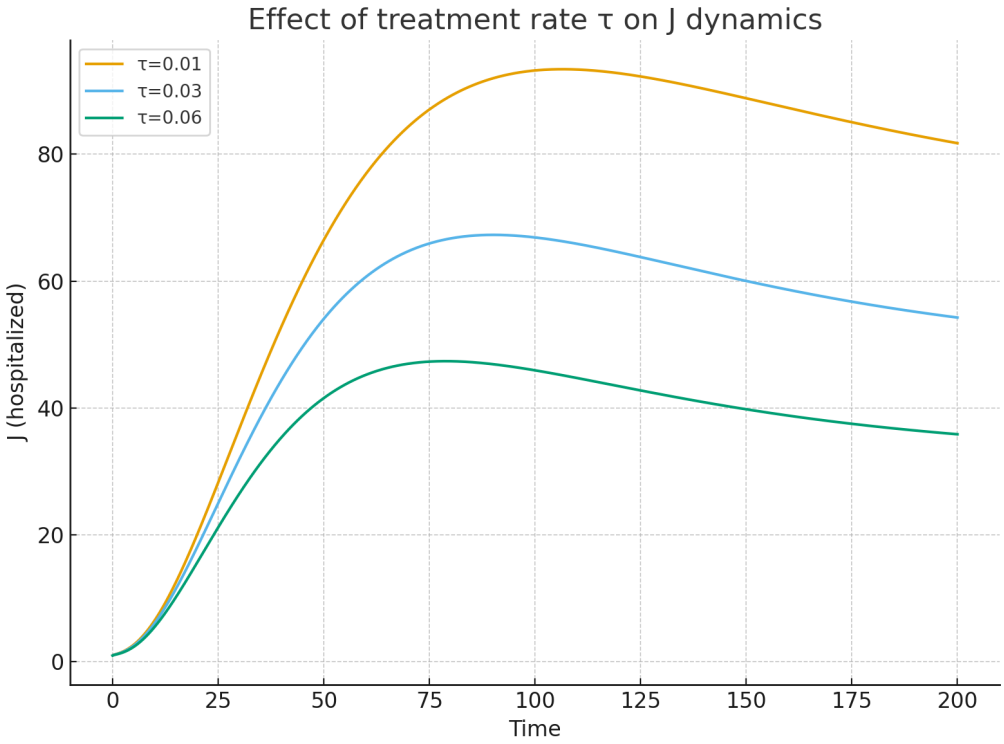

Figure 9: Effect of treatment rate τ on the hospitalized class J.

5 Conclusion

We presented a Caputo fractional-order model for the transmission dynamics of mpox in Nigeria and demonstrated its effectiveness in fitting real epidemic data. The existence and uniqueness of solutions were established under Lipschitz continuity and boundedness conditions, ensuring theoretical validity of the model. Numerical simulations using the corrected fractional Adams–Bashforth–Moulton method revealed excellent agreement with Nigeria's weekly confirmed case data.

Importantly, the estimated fractional order $\alpha^* \approx 0.215$ suggests that memory effects play a crucial role in mpox dynamics, distinguishing it from classical integer-order formulations. Our analysis further showed that increasing vaccination and quarantine rates significantly reduces the effective reproduction number R_0, thereby curtailing disease transmission.

The fractional framework thus provides not only a more accurate description of mpox dynamics but also a valuable tool for optimizing public health strategies. Future work may extend this approach to stochastic fractional models, multi-region coupling, and uncertainty quantification of fractional parameters. Overall, this study underscores the importance of fractional calculus in epidemiological modeling and its potential for enhancing preparedness and response to emerging infectious diseases.

6 Acknowledgement

The authors would like to express their sincere gratitude to all colleagues who provided valuable comments and insights during the development of this study. The authors also thank the researchers whose work in fractional calculus and epidemiological modeling has contributed to the foundations of this study.

This research received no specific grant from any funding agency in the public, commercial, or not-for-profit sectors.

References

Ahmad, Y.U., Andrawus, J., Ado, A., Maigoro, Y.A., Yusuf, A., Althobaiti, S., & Mustapha, U.T. (2024). Mathematical modeling and analysis of human-to-human monkeypox virus transmission with post-exposure vaccination. *Modeling Earth Systems and Environment*, 1–21.

Ackora-Prah, J., Koomson, A., Otoo, R.K., & Oduro, F.T. (2023). Fractional-order monkeypox virus model with sensitivity and stability analysis. *Results in Nonlinear Analysis*, *6*(4), 100–115. https://doi.org/10.53006/rna.1480887

Al Qurashi, M., Rashid, S., Alshehri, A.M., Jarad, F., & Safdar, F. (2023). New numerical dynamics of the fractional monkeypox virus model transmission pertaining to nonsingular kernels. *Mathematical Biosciences and Engineering*, *20*(1), 402–436. https://doi.org/10.3934/mbe.2023019

Al-Shomrani, M.M., Musa, S.S., & Yusuf, A. (2023). Unfolding the transmission dynamics of monkeypox virus: An epidemiological modeling analysis. *Mathematics*, *11*(5), 1121.

Andrawus, J., Ahmad, Y.U., Andrew, A.A., et al. (2025). Impact of surveillance in human-to-human transmission of monkeypox virus. *European Physical Journal Special Topics*, *234*, 483–514. `https://doi.org/10.1140/epjs/s11734-024-01346-5`

Diethelm, K. (2010). *The Analysis of Fractional Differential Equations: An Application-Oriented Exposition Using Differential Operators of Caputo Type*. Springer, Berlin.

Diethelm, K., Ford, N.J., & Freed, A.D. (2002). A predictor–corrector approach for the numerical solution of fractional differential equations. *Nonlinear Dynamics*, *29*(1–4), 3–22.

Ford, N.J., Simpson, A.C. (2001). The numerical solution of fractional differential equations: Speed versus accuracy. *Numerical Algorithms*, *26*(4), 333–346.

Gasimov, Y.S., Napoles-Valdes, J.E. (2022). Some refinements of Hermite-Hadamard inequality using k-fractional Caputo derivatives. Fractional Differential Calculus, 12(2), 209-21.

Garrappa, R. (2009). On some explicit Adams multistep methods for fractional differential equations. *Journal of Computational and Applied Mathematics*, *229*(2), 392–399.

Grant, R., Nguyen, L.B.L., & Breban, R. (2020). Modelling human-to-human transmission of monkeypox. *Bulletin of the World Health Organization*, *98*(9), 638. https://doi.org/10.2471/BLT.19.242347

Khan, S.U., Ullah, S., Li, S., Mostafa, A.M., Bilal Riaz, M., AlQahtani, N.F., & Teklu, S.W. (2024). A novel simulation-based analysis of a stochastic HIV model with time delay using high-order spectral collocation technique. *Scientific Reports*, *14*(1), 7961.

Kilbas, A.A., Srivastava, H.M., & Trujillo, J.J. (2006). *Theory and Applications of Fractional Differential Equations*. Elsevier, Amsterdam.

Kirci, O., Pandir, Y., Latifa, A., & Bulut, H. (2024). A new version of trial equation method for a complex nonlinear system arising in optical fibers. *Optical and Quantum Electronics, 56*(6), 1019.

Li, C., Zeng, F. (2020). *Numerical Methods for Fractional Calculus*. CRC Press, Boca Raton.

Li, S., Samreen, Ullah, S., Riaz, M.B., Awwad, F.A., & Teklu, S.W. (2024). Global dynamics and computational modeling approach for analyzing and controlling alcohol addiction using a novel fractional and fractal–fractional modeling approach. *Scientific Reports*, *14*(1), 5065.

Liu, B., Farid, S., Ullah, S., Altanji, M., Nawaz, R., & Teklu, S.W. (2023). Mathematical assessment of monkeypox disease with the impact of vaccination using a fractional epidemiological modeling approach. *Scientific Reports*, *13*(1), 13550. https://doi.org/10.1038/s41598-023-40745

Michael, U. E., Omenyi, L. O., Kafayat, E., Nwaeze, E., Akachukwu, O. A., Ozoigbo, G., & Ekhator, M. (2023). Monkeypox mathematical model with surveillance as control. *Communications in Mathematical Biology and Neuroscience*, 2023, Article–ID.

Nigeria Center for Disease Control and Prevention. (2023). *An Update of Monkeypox Outbreak in Nigeria.* https://ncdc.gov.ng/diseases/sitreps/?cat=8&name=An%20Update%20of%20Monkeypox%20Outbreak%20in%20Nigeria

Nolen, L.D., Osadebe, L., Katomba, J., Likofata, J., Mukadi, D., Monroe, B., ... & Reynolds, M.G. (2016). Extended human-to-human transmission during a monkeypox outbreak in the Democratic Republic of the Congo. *Emerging Infectious Diseases*, *22*(6), 1014.

Podlubny, I. (1999). *Fractional Differential Equations.* Academic Press, San Diego.

Van De Driessche, P., Watmough, J. (2002). Reproduction number and sub-threshold endemic equilibrium for compartmental models of disease transmission. *Mathematical Biosciences*, *180*, 29–48.

World Health Organization. (2022). *Strategic Preparedness, Readiness and Response Plan: Monkeypox.* https://www.who.int/publications/m/item/monkeypox-strategic-preparedness--readiness--and-response-plan-(sprp)

World Health Organization. (2023). *Multi-country Outbreak of Mpox: External Situation Report #28 – 19 September 2023.* ttps://www.who.int/publications/m/item/multi-country-outbreak-of-mpox--external-situation-report-28---19-september-2023